metals

MDPI

Article

Optimization of a Solution Treatment in the Al-Cu-Mg-Ag Alloy via a Microstructural Investigation

Hyeongsub So [1,2], Jae-Hong Shin [1], Leeseung Kang [1], Chanuk Jeong [3] and Kyou-Hyun Kim [1,*]

[1] Korea-Russia Innovation Center, Korea Institute of Industrial Technology, Incheon 22004, Korea; ksd8262@kitech.re.kr (H.S.); shinclusion@kitech.re.kr (J.-H.S.); leeseung@kitech.re.kr (L.K.)
[2] Department of Materials Science and Engineering, Korea University, Seoul 02841, Korea
[3] R&D Center, Dongyang A.K Korea Co., Ltd., Sejong 30067, Korea; rndcuj@akglobal.net
* Correspondence: khkim1308@kitech.re.kr; Tel.: +82-32-458-5127

Abstract: We investigated the effect of solution temperature ($T_{sol.}$ = 440–530 °C) on the mechanical properties of the Al–3.4Cu–0.34Mg–0.3Mn–0.17Ag alloy, finding that the investigated Al alloy showed the highest mechanical strength of σ_{UTS} = ~329 MPa at a $T_{sol.}$ value of 470 °C. The microstructural investigation demonstrates that the mechanical properties for different $T_{sol.}$ values stem from grain growth, precipitation hardening, and the formation of large particles at the grain boundaries. On the basis of $T_{sol.}$ = 470 °C, the effect of each microstructural evolution is significantly different on the mechanical properties. In this study, the relationships between the microstructural evolution and the mechanical properties were investigated with respect to different values of $T_{sol.}$

Keywords: aluminum alloy; mechanical properties; microstructural evolution; solutionization

Citation: So, H.; Shin, J.-H.; Kang, L.; Jeong, C.; Kim, K.-H. Optimization of a Solution Treatment in the Al-Cu-Mg-Ag Alloy via a Microstructural Investigation. *Metals* **2022**, *12*, 66. https://doi.org/10.3390/met12010066

Academic Editor: Andrey Belyakov

Received: 30 November 2021
Accepted: 26 December 2021
Published: 29 December 2021

1. Introduction

High-strength Al–Cu (5.0 wt.% < Cu < 7.0 wt.%)–Mg–Ag-based alloys have been widely used owing to their excellent mechanical strength with the advantage of mass production [1–5]. To obtain high mechanical properties, Al–Cu–Mg alloys require post-treatment processes, such as a heat treatment and plastic working. Al 2xxx alloys are, in general, employed via several steps, including (1) casting, (2) homogenization, (3) hot-rolling, (4) a solution treatment, (5) cold-rolling, and (6) artificial aging [5–8]. The conditions of each step are also optimized based on the compositions of the Al alloys.

Among several post-treatment processes, the solution treatment and artificial aging are of considerable importance to strengthen Al–Cu–Mg alloys by the formation of precipitates in the Al matrix [8–12]. The solution treatment process serves to induce the state of supersaturated solid solution (SSSS), which re-dissolves second phases into the matrix. Hence, the solution treatment temperature is determined based on minor elements added to Al. In Al–Cu–Mg-based alloys, the major second phases formed by minor elements are known to be intermetallic compounds of Al_2Cu and Al–Cu–Mn–Fe [13–17]. From the conventional binary phase diagram of Al–Cu, the melting temperature of the Al–Cu (5.0 wt.% < Cu < 7.0 wt.%) binary phase is approximately 550 °C. Most high-strength Al–Cu–Mg-based alloys are thus solution-treated at ~530 °C [2,3,7,10,18], while the maximum solubility of Cu to Al is only 5.57 wt.% Cu. Therefore, the solution treatment temperature is not high enough to re-dissolve the Cu minor elements into the Al matrix if the Cu content is higher than 5.57 wt.%. An insufficient solution temperature induces the residual second phase particles in the grain boundaries of Al, leading to the insufficient formation of precipitates in the Al matrix during the artificial aging process. Additionally, large particles remain in the grain boundaries due to the insufficient solution treatment temperature. It is well known that large particles in grain boundaries act as crack initiation sites, resulting in an increase in the brittleness [6,19,20].

On the other hand, the conventional solution treatment temperature of Al 2xxx alloys with 5.0 wt.% < Cu < 7.0 wt.% is high enough to induce the grain growth of Al grains. As shown in Figure 1, in the Al 2139 (Al-5.0Cu-0.50Mg) alloy, the grain growth is observed after a solution treatment at 530 °C. The mechanical strength is inversely proportional to the grain size. The grain growth of the Al matrix, therefore, should be suppressed to achieve the maximum mechanical strength.

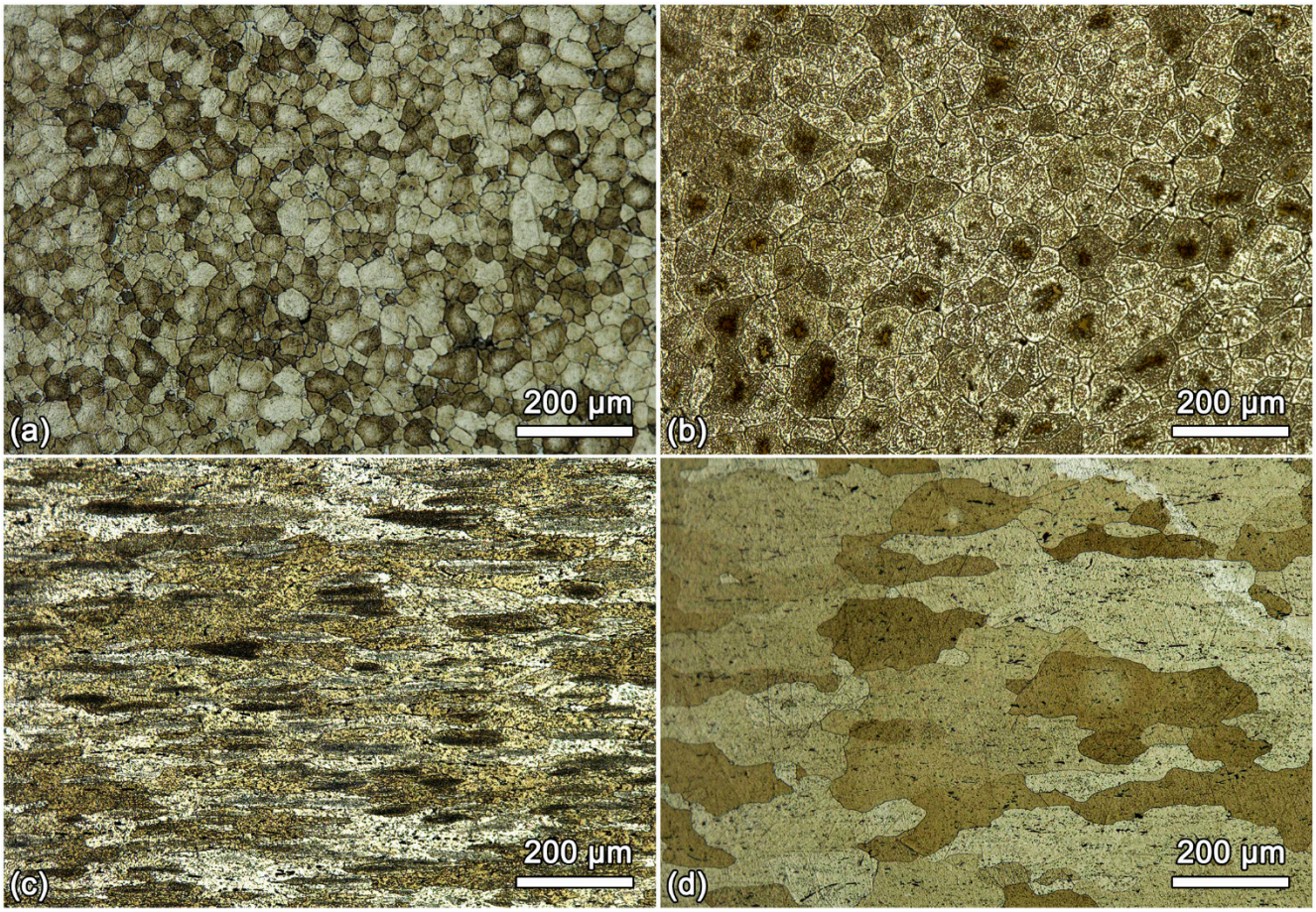

Figure 1. Microstructural investigations of each process of the Al–5.0Cu–0.50Mg–0.3Mn–0.17Ag commercial alloy: (**a**) as-cast, (**b**) homogenized, (**c**) hot-rolled, and (**d**) solutionized. This alloy is homogenized at 530 °C for 24 h, solution treated at 530 °C for 3 h, and aged at 160 °C for 24 h with the rolling processes.

Given the above considerations, the temperature range of the solution treatment for Al–Cu–Mg-based (2xxx) alloys is very limited compared to those of other heat-treatable Al alloys, such as Al–Zn–Mg-based (7xxx) alloys. For example, the maximum solubility of Zn and Mg with regard to Al is 83.1 wt.% at 381 °C and 17.1 wt.% at 450 °C, respectively. The solution temperatures are far too low to induce grain growth during the solution treatment process, while the solubility can reach the maximum level [21–24]. Thus, 7xxx series Al alloys provide a wide range of solution temperatures to optimize the mechanical properties. This then motivates careful study to determine the optimum solution treatment temperature to achieve the maximum mechanical properties of Al–Cu–Mg-based (2xxx) alloys.

In this study, we demonstrated the effect of the solution treatment temperature on the microstructures of the Al–Cu–Mg–Mn–Ag alloy resulting in a change of the mechanical properties. For the alloy design, we fabricated the Al–3.4Cu–0.34Mg–0.3Mn–0.17Ag alloy in order to investigate the wide temperature range for the solution treatment process. The maximum solid solution state can be achieved at 470 °C, which is far below the melting temperature of Al. Hence, the fabricated Al alloy samples underwent a solution treatment

at 440 °C, 470 °C, 500 °C, and 530 °C. The solid solution state and its effect on the formation of precipitates in the Al matrix were mainly investigated at the solution temperatures of 440 °C and 470 °C. For the other conditions, the effect of the grain growth was considered because the maximum solid solubility of Cu is above 470 °C. Thus, this study provides a strategy by which to optimize the conditions of the solution treatment in order to develop a high-strength Al–Cu-Mg-based alloy.

2. Experimental Procedures

By using a gravity casting, the Al–3.4Cu–0.34Mg–0.3Mn–0.17Ag alloy was prepared with high-purity elements (Al, Cu, Mg, and Ag) and master alloys (Al-15 wt.% Mn and Al-10 wt.% Ti). All components were melted using an electric resistance furnace at 800 °C, with the temperature held at this point for 30 min. Thermo-mechanical processes were determined based on the conventional conditions as shown in Figure 2 [6,12,25–27]. The as-cast samples were homogenized at 530 °C for 24 h and cooled in air. The homogenized samples were then cut into thick plates (120 × 40 × 30 mm) for a rolling process. In the synthesized Al alloy, the maximum solubility of Cu in the Al matrix was achieved at around 550 °C, while the melting temperature was 582 °C with 3.375 wt.% Cu. Thus, the plates were solutionized at 440 °C, 470 °C, 500 °C, and 530 °C for 3 h and quenched with water after the first hot rolling step. The solution temperatures used here are 80%, 85.5%, 90.9%, and 96.3% of the melting temperature of Al. For the different solution treatment temperatures ($T_{sol.}$), hereinafter, the specimens will be referred to correspondingly as sample I, sample II, sample III, and sample IV. Finally, the solutionized plates were cold-rolled under rolling reduction of 10% along the rolling direction and artificially aged in a muffle furnace at 160 °C for 24 h by a single-step aging treatment.

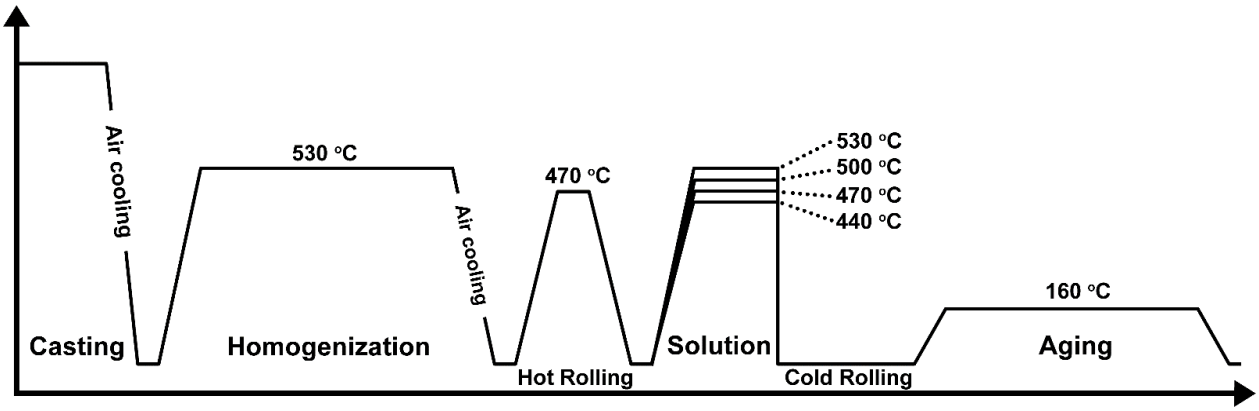

Figure 2. Schematic diagram of the applied tempering process.

Tensile tests were then done using ASTM E8 sub-size standard specimens with a total length, gage length, width, and thickness of 100 mm, 25 mm, 6 mm, and 2.5 mm, respectively [28]. The tensile properties were then measured more than ten times for each specimen using a precision universal testing machine (AGX-V, SHIMADZU, Kyoto, Japan) with a strain rate of 2 mm/min under ambient temperature conditions. The microstructures of the Al alloys were investigated from the macroscopic scale (few tens μm to ~hundreds μm) to the microscopic scale (few tens μm~nm). For the macroscopic observations using an optical microscope (OM), the specimens were mechanically mirror-polished and chemically etched with a proper etchant (95.5% water, 2% HNO_3, 1.5% HCl, 1% HF). Details of the chemical composition and overall phase identification were determined with a field emission scanning electron microscope (FE-SEM, JSM-7100F, JEOL, Kyoto, Japan) and by an energy dispersive X-ray microanalysis (EDSX, X-max, Oxford, UK). For the microscopic structural investigation, the specimens were mechanically polished down to ~10 μm and Ar-ion milled at an incident angle of 6° with an accelerating voltage of 3.0 keV to ensure electron transparency. The ultra-thin specimens were then investigated

using field-emission transmission electron microscopy (FE-TEM, JEM-ARM200F, JEOL Ltd., Tokyo, Japan) at room temperature.

3. Results and Discussion

Figure 3 shows the tensile properties of Al–3.4Cu–0.34Mg–0.3Mn–0.17Ag for different values of $T_{sol.}$. The mechanical properties of sample I were determined to be σ_y = 261 ± 4.25 MPa and σ_{UTS} = 329 ± 8.17 MPa with an ε (elongation) rate of 13.1 (±0.29)%. As shown in Figure 3, the tensile stress gradually increased as $T_{sol.}$ increased. The maximum tensile stress was achieved when $T_{sol.}$ was 470 °C (sample II), while the elongation was slightly reduced to ~ 12.1 (±0.49)%. The tensile stress was then degraded when $T_{sol.}$ exceeded 470 °C. The tensile stresses were found to be 279 ± 7.09 MPa (σ_y) and 346 ± 9.87 MPa (σ_{UTS}) for sample III and ~258 ± 8.94 MPa (σ_y) and ~326 ± 7.08 MPa (σ_{UTS}) for sample IV. In contrast, the elongation outcomes increased sharply as follows: 15.2 (±0.56)% (sample III) → 16.7 (±0.68)% (sample IV).

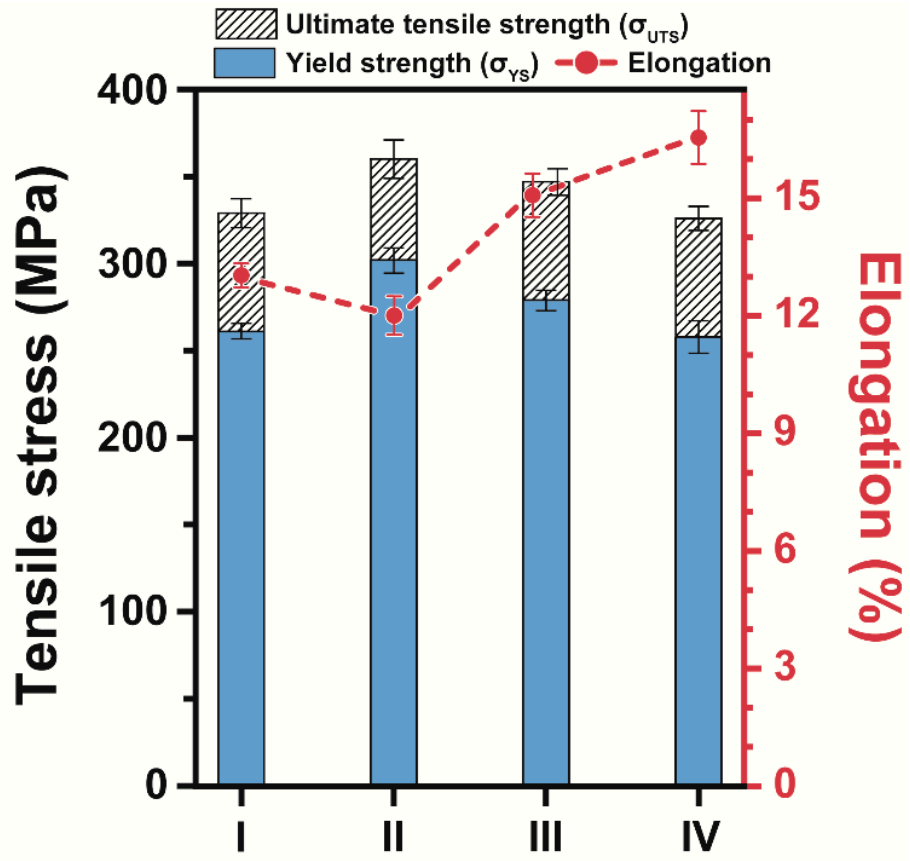

Figure 3. Tensile properties of the synthesized alloys with respect to the various values of $T_{sol.}$.

Figure 4 shows typical OM images of samples I–IV observed along the rolling direction (RD) of the cold-rolled (CR) specimens. In order to observe the change in the grain size, the OM images were recorded from approximately 30 different regions of each sample and averaged, as presented in Figure 4e. Figure 4e shows that the average grain sizes gradually increased by ~98 (±25.7) μm (sample I) → ~131 (±25.0) μm (sample II) → ~181 (±34.6) μm (sample III) → ~203 (±46.9) μm (sample IV) as $T_{sol.}$ increased. It can be clearly observed that the grain size of Al was highly sensitive to $T_{sol.}$. In addition, the investigated range of $T_{sol.}$ from 440 °C to 530 °C was sufficient to induce grain growth at the Al matrix of Al–3.4Cu–0.34Mg–0.3Mn–0.17Ag. In general, the grain size is inversely proportional to the mechanical strength. As shown in Figure 4, however, the tensile stress of sample II was enhanced compared to that of sample I, while the average grain size of sample II was much larger than the grain size of sample I. In contrast, the tensile stresses of sample III and IV

decreased drastically compared to that of sample II, identical to the variations of the grain size shown in Figure 4. A discussion of these findings with regard to the microstructural changes is provided later in the paper.

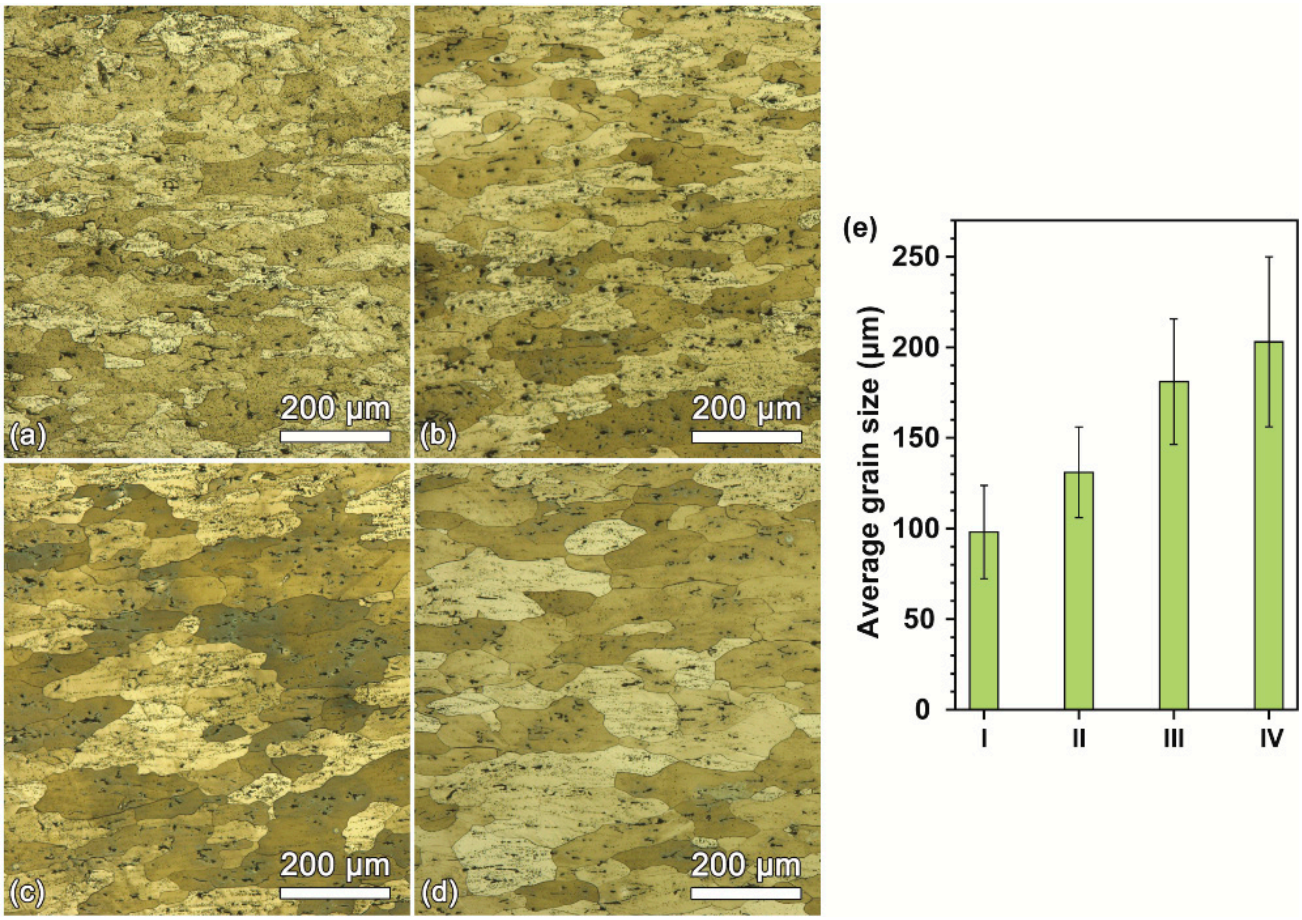

Figure 4. OM microstructures of (**a**) sample I, (**b**) sample II, (**c**) sample III, and (**d**) sample IV. The average grain sizes are provided in (**e**) with the error bar.

Figure 5 shows backscattered electron micrographs (BSE) of the synthesized alloys recorded along the rolling direction (RD). Two different phases were clearly observed in the grain boundary regions, as indicated by the arrows I and II in Figure 5. A chemical analysis then revealed that the corresponding particles, which formed in the grain boundaries, are the Al–Cu–Mn–Fe (yellow arrow) and Al_2Cu (black arrow) phases, which are in general observed in Al–Cu–Mg–Ag alloys [13–17]. During the solution treatment process, solute atoms were dissolved into the Al matrix to generate SSSS, which resulted in the formation of strengthening phases in the Al matrix after the artificial aging process. Macroscopically, the average particle sizes of Al–Cu–Mn–Fe and Al_2Cu simultaneously decreased by ~23.5 ± 6.38 μm (sample I) → ~18.3 ± 6.64 μm (sample II) → ~12.36 ± 3.94 μm (sample III) → ~6.76 ± 1.18 μm (sample IV) as $T_{sol.}$ increased. In addition to the decrease in the particle size, Figure 6 shows the changes of the area fractions of Al–Cu–Mn–Fe and Al_2Cu particles with respect to $T_{sol.}$. The average area fractions of Al_2Cu particles in each alloy were determined to be by 1.10, 1.09, 0.89, and 0.49%. Additionally, the area fractions of Al–Cu–Mn–Fe particles were found to be 3.53, 1.51, 0.52, and 0.25%. Regarding the solubility of the constituent elements in the Al matrix, Table 1 shows that the major element of Cu gradually increased as $T_{sol.}$ increased. On the other hand, the increased level of Cu elements in the Al matrix facilitated the formation of major hardening precipitates of Al_2Cu after the artificial aging process. The tensile stress of synthesized alloys, however, reached its maximum at a $T_{sol.}$ value of 470 °C, while the minimum particle size and the maximum

Cu solubility were both achieved at a $T_{sol.}$ value of 530 °C. Moreover, the mechanical strength gradually decreased as $T_{sol.}$ exceeded 470 °C, while the elongation increased drastically. For heat-treatable Al alloys, the formation of hardening phases in the Al matrix is mostly subject to the mechanical properties. A nanoscopic structure investigation using TEM was therefore conducted in order to investigate the behavior of the formation of the hardening phases.

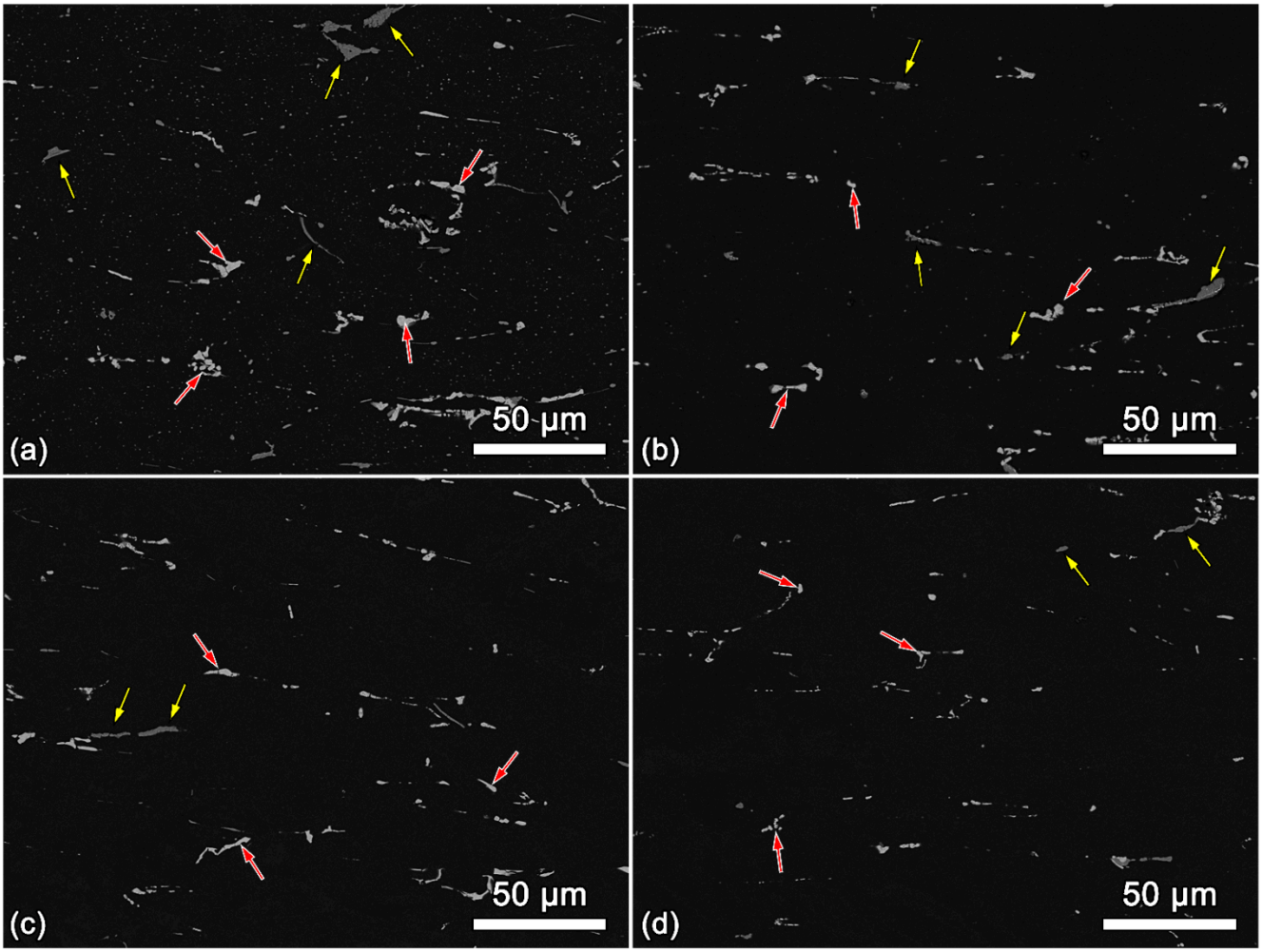

Figure 5. Backscattered electron microscopy recorded from (**a**) sample I, (**b**) sample II, (**c**) sample III, and (**d**) sample IV. Two coarse phases are pointed with yellow arrow (Al–Cu–Mn–Fe) and red arrow (Al_2Cu).

Table 1. Chemical composition (at.%) in the Al matrix of the aged Al–Cu–Mg–Mn–Ag alloys.

Alloys	Cu	Mg	Mn	Ag	Al
Sample I	2.71(±0.08)	0.33(±0.08)	0.18(±0.01)	0.23(±0.02)	Bal.
Sample II	3.32(±0.24)	0.27(±0.09)	0.29(±0.03)	0.09(±0.02)	Bal.
Sample III	3.45(±0.05)	0.29(±0.05)	0.35(±0.04)	0.10(±0.01)	Bal.
Sample IV	3.60((±0.23)	0.30(±0.08)	0.34(±0.02)	0.06(±0.02)	Bal.

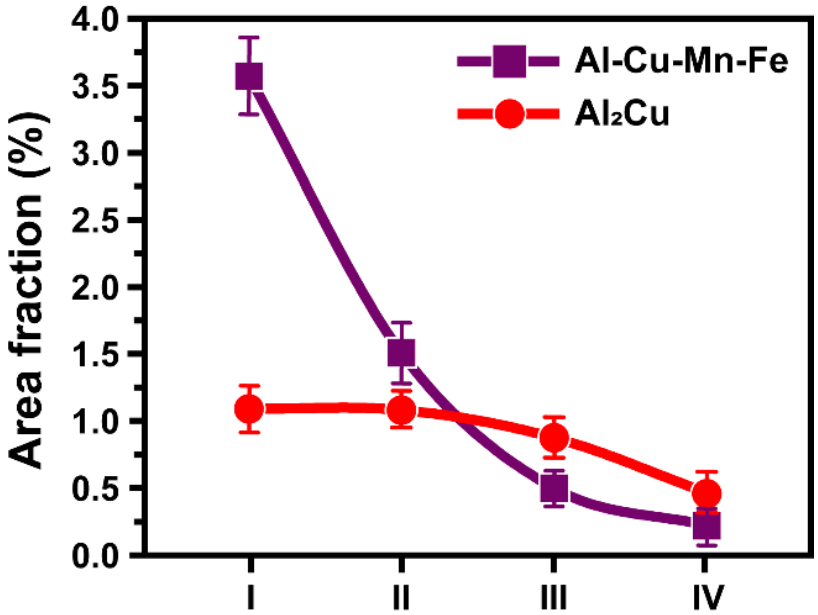

Figure 6. Area fractions of second phases in the synthesized Al alloys.

Figure 7 presents typical TEM micrographs of samples I–IV recorded under medium magnification with the corresponding spot electron diffraction (ED) patterns. TEM investigations were performed in all cases along the zone axis of $\{110\}_{Al}$, which is the optimum direction at which to investigate the hardening phases of θ′ and Ω. From earlier reports, it is well known that the θ′ and Ω phase are respectively lied on {002} and {111} [2,7,9,29,30]. Figure 7e shows the number density of precipitates calculated from each specimen. For sample I, the number density was about 89.49(±27.25)/μm^2. This value was similar to that of sample II (114.25(±44.90)/μm^2), though $T_{sol.}$ increased. The formation of hardening phases, however, was drastically enhanced in sample II. The calculated number densities of the precipitates were 173.91(±37.19)/μm^2 and 358.43(±63.52)/μm^2 for sample III and sample IV, respectively. The drastic increase in the hardening phases could also be confirmed in the spot ED patterns. As shown in the inset of Figure 7a,b, samples I and II consisted of Al Bragg spots for the zone axis of $\{110\}_{Al}$ without any evidence of hardening phases in the Al matrix. In contrast, coherently formed hardening phases were well-observed as streaks along the $\{110\}_{Al}$ and $\{002\}_{Al}$ directions in the spot ED patterns of samples III and IV (Figure 7c,d). On the other hand, the variations in the number densities were nearly identical to the content of Cu solute elements in the Al matrix, as shown in Figure 7e. Interestingly, the number density of the hardening phases was highly sensitive to the Cu solute atoms when $T_{sol.}$ exceeded 470 °C, where 3.4 wt.% Cu was entirely solutionized in the binary phase diagram of Al–Cu. The amount of Cu solute (at.%), presented in Table 1, increased by ~125% from sample I to sample II. In contrast, the increment of Cu solute was only a few percent when the $T_{sol.}$ was greater than 470 °C. This suggests that $T_{sol.}$ was not the only consideration to achieve the maximum solubility of major solute elements in order to facilitate the formation of a hardening phase.

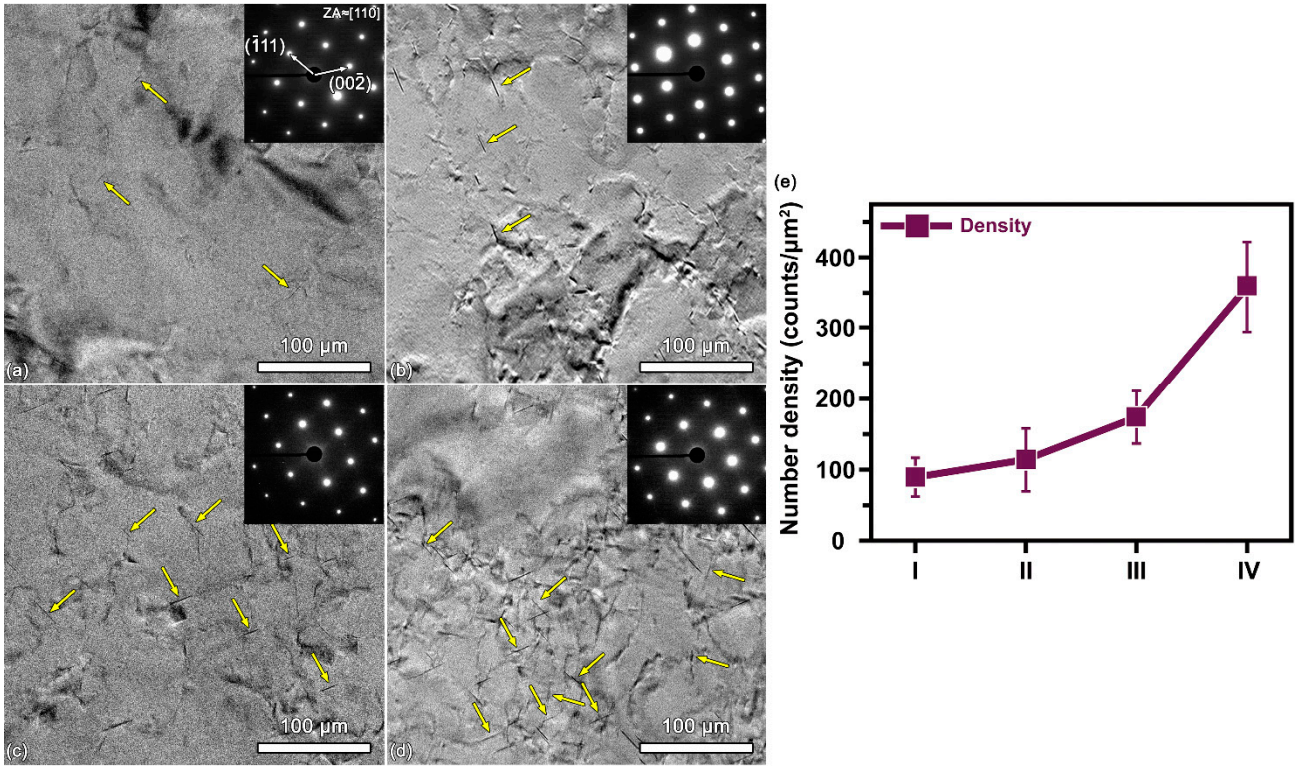

Figure 7. (**a**–**d**) Medium-magnification BF images and corresponding electron diffraction results recorded at the $\{110\}_{Al}$ zone axis: (**a**) sample I, (**b**) sample II, (**c**) sample III, (**d**) sample IV, and (**e**) number density of hardening phases (θ′ and Ω) with respect to $T_{sol.}$.

Considering the above findings, $T_{sol.}$ affects the mechanical properties of the Al–Cu–Mg–Ag alloy in terms of three microstructural aspects. First, the tensile stress was mainly determined by the number density of the hardening precipitates (θ′ and Ω) from 440 °C to 470 °C. For this $T_{sol.}$ range, the OM images indicate that the Al grains grew significantly by ~140% (98 μm → 131 μm). Nevertheless, the tensile stress was improved from σ_{UTS} = 329 MPa to σ_{UTS} = 360 MPa. The binary phase diagram of Al–Cu indicated that 3.4 wt.% Cu had maximum solubility above a $T_{sol.}$ value of approximately 470 °C as proven by a chemical analysis (Table 1). In consequence, an increase in the Cu solubility level in Al (Table 1) facilitated the formation of hardening precipitates (θ′ and Ω) in the Al matrix, which improved the tensile stress.

Second, the mechanical properties were affected by the grain growth at $T_{sol.}$ of 470 °C. At the $T_{sol.}$ value of ~500–530 °C, the Cu solute in the Al matrix was mostly saturated. The number density of the hardening precipitates reached its maximum of 358.43 counts/μm^2 at $T_{sol.}$ of 530 °C, while the tensile stresses were gradually reduced to 326 MPa. This is considered to be a result of the growth of Al grains. The Al grain size increased to 203 μm at 530 °C, while the initial Al grain size was 98 μm. That is, the grain size of Al mainly determined the mechanical properties of the Al–Cu–Mg–Ag alloy once the Cu solute was maximized.

Finally, the elongation of the investigated alloys was primarily determined by the large particles that formed at the grain boundaries. As shown in Figure 5, large particles formed at the grain boundaries of the Al–3.4Cu–0.34Mg–0.3Mn–0.17Ag alloy. The large particles were then finely distributed as $T_{sol.}$ increased. The area fractions of the large particles (Al–Cu–Mn–Fe and Al_2Cu) abruptly decreased and reached their minimum value at the highest $T_{sol.}$ level of 530 °C. In general, large particles are known to act as crack initiation and development sites [6,20]. Consequently, a decrease in the number of large particles resulted in an increase in the elongation in the Al–3.4Cu–0.34Mg–0.3Mn–0.17Ag alloy.

4. Conclusions

We investigated the microstructural evolution of the Al–3.4Cu–0.34Mg–0.3Mn–0.17Ag alloy with respect to a wide range of $T_{sol.}$ values. Interestingly, in this study, the mechanical properties of the Al–Cu–Mg–Ag alloy were determined by several factors according to the solution temperature ($T_{sol.}$). The used $T_{sol.}$ could then be divided into three ranges based on the Cu solid solution: (1) an insufficient solution temperature range ($T_{sol.}$ < 470 °C), (2) a sufficient solution temperature range ($T_{sol.}$ ≈ 470 °C), and (3) a high solution temperature range ($T_{sol.}$ > 470 °C). For the first temperature range of 440 °C < $T_{sol.}$ < 470 °C, the amount of Cu solute increased in the Al matrix to facilitate the formation of hardened nanoprecipitates (θ′ and Ω). This then resulted in an improvement of the tensile stress while grain growth was observed. For the next temperature range of $T_{sol.}$ > 470 °C, the number density of hardening precipitates was maximized. Nevertheless, the grain growth acted as a dominant factor to lower the tensile stress of the synthesized alloys, unlike in the first temperature range of 440 °C < $T_{sol.}$ < 470 °C. On the other hand, the decrease of the volume fraction of the large particles helped to improve the ductility of the synthesized alloys. Based on the above, therefore, the solution temperatures should be properly controlled to (1) optimize the microstructural evolutions of the grain growth of Al, to (2) decrease the number of large particles, which form at the grain boundaries, and to (3) facilitate the hardening of precipitates of Al_2Cu in order to optimize the mechanical properties of Al–Cu–Mg–Ag alloys.

Author Contributions: Conceptualization, H.S.; investigation, H.S. and C.J.; data curation, H.S.; writing—original draft preparation, H.S.; writing—review and editing, J.-H.S., L.K. and K.-H.K.; project administration, K.-H.K.; resources, J.-H.S.; supervision, L.K.; funding acquisition, K.-H.K. All authors have read and agreed to the published version of the manuscript.

Funding: This research was financially supported by the Institute of Civil Military Technology Cooperation funded by the Defense Acquisition Program Administration and by the Ministry of Trade, Industry, and Energy of the Korean government under Grant No. UM21308RD3. This study was also equally supported by the R&D program from the Korea Institute of Industrial Technology.

Institutional Review Board Statement: Not applicable.

Informed Consent Statement: Not applicable.

Data Availability Statement: The raw/processed data required to reproduce these findings cannot be shared at this time as the data also forms part of an ongoing study.

Conflicts of Interest: The authors declare no conflict of interest.

References

1. Xiao, D.H.; Wang, J.N.; Ding, D.Y.; Chen, S.P. Effect of Cu content on the mechanical properties of an Al-Cu-Mg-Ag alloy. *J. Alloys Compd.* **2002**, *343*, 77–81. [CrossRef]
2. Polmear, I.J.; Pons, G.; Barbaux, Y.; Octor, H.; Sanchez, C.; Morton, A.J.; Borbidge, W.E.; Rogers, S. After Concorde: Evaluation of creep resistant Al-Cu-Mg-Ag alloys. *Mater. Sci. Technol.* **1999**, *15*, 861–868. [CrossRef]
3. Xiao, D.H.; Wang, J.N.; Ding, D.Y.; Yang, H.L. Effect of rare earth Ce addition on the microstructure and mechanical properties of an Al-Cu-Mg-Ag alloy. *J. Alloys Compd.* **2003**, *352*, 84–88. [CrossRef]
4. Gazizov, M.; Teleshov, V.; Zakharov, V.; Kaibyshev, R. Solidification behaviour and the effects of homogenisation on the structure of an Al-Cu-Mg-Ag-Sc alloy. *J. Alloys Compd.* **2011**, *509*, 9497–9507. [CrossRef]
5. Zuiko, I.; Kaibyshev, R. Effect of plastic deformation on the ageing behaviour of an Al-Cu-Mg alloy with a high Cu/Mg ratio. *Mater. Sci. Eng. A* **2018**, *737*, 401–412. [CrossRef]
6. So, H.; Won, S.J.; Park, J.; Oh, S.J.; Kang, L.; Kim, K.H. Mechanical properties and microstructural evolution in Al-Cu-Mg-Ag alloy with a $Cu_xMg_{x/10}$ content. *Mater. Sci. Eng. A* **2021**, *824*, 141573. [CrossRef]
7. Lumley, R.N.; Morton, A.J.; Polmear, I.J. Enhanced creep performance in an Al-Cu-Mg-Ag alloy through underageing. *Acta Mater.* **2002**, *50*, 3597–3608. [CrossRef]
8. Marceau, R.K.W.; Sha, G.; Ferragut, R.; Dupasquier, A.; Ringer, S.P. Solute clustering in Al-Cu-Mg alloys during the early stages of elevated temperature ageing. *Acta Mater.* **2010**, *58*, 4923–4939. [CrossRef]
9. Gable, B.M.; Shiflet, G.J.; Starke, E.A. Alloy development for the enhanced stability of Omega precipitates in Al-Cu-Mg-Ag alloys. *Metall. Mater. Trans. A* **2006**, *37A*, 1091–1105. [CrossRef]

10. Liu, X.Y.; Pan, Q.L.; Lu, Z.L.; Cao, S.F.; He, Y.B.; Li, W.B. Effects of solution treatment on the microstructure and mechanical properties of Al-Cu-Mg-Ag alloy. *Mater. Des.* **2010**, *31*, 4392–4397. [CrossRef]
11. Ibrahim, M.F.; Samuel, A.M.; Samuel, F.H. A preliminary study on optimizing the heat treatment of high strength Al-Cu-Mg-Zn alloys. *Mater. Des.* **2014**, *57*, 342–350. [CrossRef]
12. Zamani, M.; Toschi, S.; Morri, A.; Ceschini, L.; Seifeddine, S. Optimisation of heat treatment of Al-Cu-(Mg-Ag) cast alloys. *J. Therm. Anal. Calorim.* **2020**, *139*, 3427–3440. [CrossRef]
13. Wang, S.C.; Starink, M.J. Precipitates and intermetallic phases in precipitation hardening Al-Cu-Mg-(Li) based alloys. *Int. Mater. Rev.* **2005**, *50*, 193–215. [CrossRef]
14. Ilevbare, G.O.; Scully, J.R. Oxygen reduction reaction kinetics on chromate conversion coated Al-Cu, Al-Cu-Mg, and Al-Cu-Mn-Fe intermetallic compounds. *J. Electrochem. Soc.* **2001**, *148*, B196–B207. [CrossRef]
15. Li, J.C.; Birbilis, N.; Buchheit, R.G. Electrochemical assessment of interfacial characteristics of intermetallic phases present in aluminium alloy 2024-T3. *Corros. Sci.* **2015**, *101*, 155–164. [CrossRef]
16. Boag, A.P.; McCulloch, D.G.; Jamieson, D.N.; Hearne, S.M.; Hughes, A.E.; Ryan, C.G.; Toh, S.K. Combined nuclear microprobe and TEM study of corrosion pit nucleation by intermetallics in aerospace aluminium alloys. *Nucl. Instrum. Methods Phys. Res. B* **2005**, *231*, 457–462. [CrossRef]
17. Alba-Galvin, J.J.; Gonzalez-Rovira, L.; Bethencourt, M.; Botana, F.J.; Sanchez-Amaya, J.M. Influence of Aerospace Standard Surface Pretreatment on the Intermetallic Phases and CeCC of 2024-T3 Al-Cu Alloy. *Metals* **2019**, *9*, 320. [CrossRef]
18. Bai, S.; Liu, Z.Y.; Gu, Y.X.; Zhou, X.W.; Zeng, S.M. Microstructures and fatigue fracture behavior of an Al-Cu-Mg-Ag alloy with a low Cu/Mg ratio. *Mater. Sci. Eng. A* **2011**, *530*, 473–480. [CrossRef]
19. Park, M.J.; So, H.; Kang, L.S.; Byeon, J.W.; Kim, K.H. The relation between mechanical properties and microstructural evolution induced by Sc microalloying in Al-20Zn-3Cu alloy. *J. Alloys Compd.* **2021**, *889*, 161719–161725. [CrossRef]
20. Zhou, Q.; Wang, J.; Misra, A.; Huang, P.; Wang, F.; Xu, K.W. Atomistic study of fundamental character and motion of dislocations in intermetallic Al_2Cu. *Int. J. Plast.* **2016**, *87*, 100–113. [CrossRef]
21. Rafi, H.K.; Ram, G.D.J.; Phanikumar, G.; Rao, K.P. Microstructure and tensile properties of friction welded aluminum alloy AA7075-T6. *Mater. Des.* **2010**, *31*, 2375–2380. [CrossRef]
22. Tian, S.K.; Li, J.Y.; Zhang, J.L.; Zhumabieke, W.; Lv, D. Effect of Zr and Sc on microstructure and properties of 7136 aluminum alloy. *J. Mater. Res. Technol.* **2019**, *8*, 4130–4140. [CrossRef]
23. Xu, D.K.; Rometsch, P.A.; Birbilis, N. Improved solution treatment for an as-rolled Al-Zn-Mg-Cu alloy. Part II. Microstructure and mechanical properties. *Mater. Sci. Eng. A* **2012**, *534*, 244–252. [CrossRef]
24. Ghiaasiaan, R.; Zeng, X.C.; Shankar, S. Controlled Diffusion Solidification (CDS) of Al-Zn-Mg-Cu (7050): Microstructure, heat treatment and mechanical properties. *Mater. Sci. Eng. A* **2014**, *594*, 260–277. [CrossRef]
25. Liu, X.Y.; Pan, Q.L.; Fan, X.; He, Y.B.; Li, W.B.; Liang, W.J. Microstructural evolution of Al-Cu-Mg-Ag alloy during homogenization. *J. Alloys Compd.* **2009**, *484*, 790–794. [CrossRef]
26. Cho, A.; Bes, B. Damage tolerance capability of an Al-Cu-Mg-Ag alloy(2139). *Mater. Sci. Forum* **2006**, *519–521*, 603–608. [CrossRef]
27. Zuiko, I.S.; Kaibyshev, R. Ageing response of cold-rolled Al-Cu-Mg alloy. *Mater. Sci. Eng. A* **2020**, *781*, 139148. [CrossRef]
28. ASTM, E. Standard Test Methods for Tension Testing of Metallic Materials; 2001. Available online: https://www.astm.org/e0008-01.html (accessed on 29 November 2021).
29. Hutchinson, C.R.; Fan, X.; Pennycook, S.J.; Shiflet, G.J. On the origin of the high coarsening resistance of Omega plates in Al-Cu-Mg-Ag alloys. *Acta Mater.* **2001**, *49*, 2827–2841. [CrossRef]
30. Ringer, S.P.; Yeung, W.; Muddle, B.C.; Polmear, I.J. Precipitate stability in Al-Cu-Mg-Ag alloys aged at high temperatures. *Acta Metal. Mater.* **1994**, *42*, 1715–1725. [CrossRef]